Research Article | Vol. 28, No. 15 / 20 July 2020 / Optics Express 21856
Optics EXPRESS

# X-ray phase-sensitive imaging using a bilens interferometer based on refractive optics

D. Zverev,[1] I. Snigireva,[2,*] V. Kohn,[3] S. Kuznetsov,[4] V. Yunkin,[4] and A. Snigirev[1]

[1]Immanuel Kant Baltic Federal University, 14 A. Nevskogo, Kaliningrad 236041, Russia
[2]European Synchrotron Radiation Facility (ESRF), 71 Avenue des Martyrs, Grenoble 38043, France
[3]National Research Centre, Kurchatov Institute, 1 Kurchatov Square, Moscow 123182, Russia
[4]Institute of Microelectronics Technology RAS, 6 Institutskiy Prospekt, Chernogolovka 142432, Russia
*snigireva@esrf.fr

**Abstract:** The phase-sensitive X-ray imaging technique based on the bilens interferometer is developed. The essence of the method consists of scanning a sample, which is set upstream of the bilens across the beam of one lens of the interferometer by recording changes in the interference pattern using a high-resolution image detector. The proposed approach allows acquiring the absolute value of a phase shift profile of the sample with a fairly high phase and spatial resolution. The possibilities of the imaging technique were studied theoretically and experimentally using fibres with different sizes as the test samples at the ESRF ID06 beamline with 12 keV X-rays. The corresponding phase shift profile reconstructions and computer simulations were performed. The experimental results are fully consistent with theoretical concepts and appropriate numerical calculations. Applications of the interferometric imaging technique are discussed, as well as future improvements.



## 1. Introduction

Nowadays, the continuous evolution of synchrotron radiation sources has resulted in a dramatic increase of brilliance and degree of spatial coherence with respect to older designs. The availability of such intense coherent X-ray beams has triggered the development of wave splitting interferometers similar to the classical double-slit Young's experiment. The spatial coherence of the X-ray source, due to its very small size, was measured in several different ways, namely with double-slits [1–4], double-mirrors [5–7] and double-prisms [8,9]. The laser-like properties of synchrotron beams enabled to develop in-line or paraxial X-ray interferometry schemes, such as those based on grating interferometers, which are used for phase-contrast imaging of objects with a micron resolution [10–12].

A bilens interferometer consisting of two parallel compound refractive lenses (CRL) was proposed [13]. Under coherent X-ray illumination, the bilens interferometer generates two diffraction-limited mutually coherent beams that are focused at some distance. When the beams overlap, they generate an interference pattern with a fringe spacing ranging from tens of nanometers to tens of micrometers, depending on the distance to the observation plane. As an evolution of such systems, a multilens interferometer, in which more than two parallel lens arrays are arranged, was demonstrated [14,15]. The enlargement of the interferometer acceptance gives rise to an increase in the contrast of the interference pattern and a narrowing of the interference fringes. The multilens arrangement substantially changes the interference pattern by adding a strong longitudinal functional dependence, which can be described using the Talbot imaging formalism. CRL-based interferometers are to fully utilize the most outstanding properties of the modern synchrotron radiation sources such as brightness, monochromaticity, and coherence to efficiently generate a periodic interference pattern in a wide range of X-ray energies.

#389940 https://doi.org/10.1364/OE.389940
Journal © 2020 Received 6 Feb 2020; revised 7 Jun 2020; accepted 17 Jun 2020; published 9 Jul 2020

Optics EXPRESS

This simple way of creating an interference pattern opens up new opportunities for the development of phase-contrast imaging techniques. For example, as in the case of classical interferometry, one can easily insert a sample upstream of one lens array of the bilens interferometer. The sample leads to a certain phase shift (delay) of the incident beam shifting the interference fringes. The high sensitivity of the interference pattern to the phase distortions of the beam produced by the sample allows extracting comprehensive information about the sample structure. To reconstruct the phase shift profile of the object, it is necessary to analyze the shifts of the interference fringes recorded during the scanning of the sample in the direction perpendicular to the optical axis.

In this paper, we demonstrate a bilens interferometer for phase-sensitive X-ray imaging of weakly absorbing materials for high energy X-rays. The interference fringe patterns were recorded experimentally when the samples were moved across the optical axis in front of a bilens interferometer. Computer simulations of interference patterns from the same objects were performed. Shifts of the interference fringes were detected and the phase shift profiles of the sample were reconstructed, which very well coincides with the calculated ones.

## 2. Theory

Let us consider the setup that involves an X-ray point source, which produces monochromatic radiation with wavelength $\lambda$, and bilens interferometer. Bilens interferometer comprises of two identical, parallel planar arrays of individual CRLs, whose optical axes are separated transversally by a distance $d$. Each CRL has the physical aperture $A$ and consists of $N$ individual double concave parabolic lenses with the radius of curvature at the parabola apex $R$. Under coherent illumination, the bilens interferometer generates two mutually coherent beams focused at some distance, which in the thin lens approximation, can be calculated as $z_f = f\, z_0 \,/\, (z_0 - f)$, where $f = R \,/\, 2N\delta$ is the lens focal length and $z_0 > f$ is the distance from the source to the bilens, $\delta$ is the decrement of the refractive index $n$ of the bilens material. The foci are spaced apart in the transverse direction by a distance $d_f = d\, z_0 \,/\, (z_0 - f)$, which tends to the value $d$, when $z_0$ is much larger than $f$.

According to the theory of wave optics, the size of each focal spot is diffraction-limited and can be estimated as $\sigma_f = \lambda\, z_f \,/\, 2A_{eff}$, where $A_{eff}$ is the effective aperture of a single CRL. It should be noted that in practice, the diffraction-limited conditions might suffer from wavefront aberrations. The effective aperture $A_{eff} \approx (\lambda f \delta \,/\, 2\beta)^{1/2}$ depends on the absorption in the bilens material, which is described by the imaginary part $\beta$ of the refraction index $n = 1 - \delta + i\beta$ [16,17]. It is assumed here that the physical aperture $A$ of each lens is larger than the effective aperture $A_{eff}$ and less than or equal to the distance $d$. It should be noted that in typical cases when the effective aperture is smaller or comparable to the physical aperture, the ratio $\sigma_f \,/\, d_f = A_{eff}\ \gamma \,/\, d$ is smaller than $\gamma = \beta \,/\, \delta$. In the hard X-ray regime, the value $\gamma$ is $10^{-2}$–$10^{-5}$ for materials that are often used for refractive optics. Therefore, the size of the focal spots is several orders of magnitude smaller than the distance between them. These focal spots can be considered as two extremely small mutually coherent secondary sources, separated in the transverse direction and generating two divergent beams, therefore this system can be described in the frame of the classical theory of in-line interferometry. According to this theory, these divergent beams generate a specific pattern of interference fringes in the area where they overlap.

For definiteness, let us consider the interferometry layout implemented at the synchrotron source when $z_0 \gg f$. The beams begin to overlap at a distance $l \approx d \,/\, \alpha$ from the foci, where $\alpha = A_{eff} \,/\, f$ is the angular size of the focused beam. Because the angle $\alpha$ for the typical X-ray CRL is small, the distance $l$ is always much larger than the space $d$ between the foci. Therefore, the paraxial approximation can be used to describe the interference of beams. Thus, at any point with a transverse coordinate $x$ in the plane of the interference pattern, observed at some distance

Optics EXPRESS

$z$ from the foci, so that $z > l \gg d$ and $x$, the intensity is expressed by the following equation:

$$I(x,z) = I_1 + I_2 + 2\sqrt{I_1 I_2}\cos\left(\frac{2\pi d}{\lambda z}x + \Delta\varphi\right), \tag{1}$$

where $I_1$ and $I_2$ are the intensities at a given point produced by each of the two waves coming from the corresponding focus, and $\Delta\varphi$ is the initial phase difference of the waves, which is equal to zero for the optical system under consideration. In general, $I_1$ and $I_2$ are different due to the Gaussian intensity distribution for both divergent beams caused by the absorption of X-rays in the CRLs. However, these intensities are almost identical at large distances $z \gg l$, where the beams completely overlap. Thus, the intensity distribution of each beam can be described by the same expression:

$$I_B(x,z) \sim \exp\left(-\frac{x^2}{2c^2}\right), \text{ where } c = \frac{A_{eff}}{(2\pi)^{1/2}}\frac{z}{f}, \tag{2}$$

The transverse size $\omega$ of the beams is equal to $(8\ln 2)^{1/2}c$ and defined as the full width at half maximum (FWHM) of their intensity distribution. Given the above, Eq. (1) can be written as:

$$I(x,z) = 2I_B(x,z)\left[1 + \cos\left(\frac{2\pi d}{\lambda z}x\right)\right]. \tag{3}$$

According to this equation, the position of interference fringes is defined by the condition $x_m = m\,\lambda z\,/\,d$, where $m$ takes integer values, while the spacing between successive maxima or period of the interference fringes is given by:

$$\Lambda = \frac{\lambda}{d}z. \tag{4}$$

Like the intensity distribution of divergent beams, the envelope of interference fringes has the Gaussian shape with the same parameter $c$, which also determines the transverse size of the interference pattern $\omega$ [see Eq. (2)]. The number of interference fringes can be estimated as $M \approx \omega\,/\,\Lambda = (4\ln 2\,/\,\pi)^{1/2}d\,/\,(2\gamma\,A_{eff})$. One can observe approximately $(2\gamma)^{-1}$ number of fringes if the effective aperture $A_{eff}$ is comparable with the distance $d$ and more fringes for smaller values of $A_{eff}$. In the field of hard X-rays, this value is quite large and can range from $10^2$ to $10^5$, depending on the material of the interferometer. The foregoing makes the use of the bilens for coherent X-ray applications very promising.

It should be noted that the above consideration is valid as well for an X-ray source with a finite size $s_0$. However, the extended source significantly affects the quality of the interference pattern, reducing the visibility of interference fringes. The visibility can be estimated from the convolution of the intensity profile expressed by the Eq. (3) with a Gaussian distribution of the intensity of the source projection in the observation plane [13]:

$$V = \exp\left[-\frac{\pi^2}{4\ln 2}\left(\frac{s_0}{\Lambda}\frac{z}{z_0}\right)^2\right]. \tag{5}$$

The equation is obtained under the approximation that $I_B$ is constant for several successive maxima, which is valid because of $\Lambda < \omega$. It can be seen that the visibility is a function of the source size, which is equal to unity for a point source and tends to zero when the size of the source projection $s_0\,z\,/\,z_0$ is larger than $\Lambda$. Therefore, the bilens interferometer can be considered as a highly sensitive tool for the source diagnostics [13].

The difference $\Delta\varphi$ in the initial phase of two beams is another parameter that has a significant impact on the generated interference pattern. As noted above, the phase difference between the two interfering beams is zero for the optical setup under consideration. However, if the sample is

Optics EXPRESS

placed in front of the bilens in one of the beams, then $\Delta\varphi$ is not zero. This phase difference leads to a shift of the interference fringes in the transverse direction by a distance equal to:

$$\Delta x = \frac{\Delta\varphi}{2\pi}\Lambda. \tag{6}$$

Tracking the shift of interference fringes in the process of scanning a sample through the bilens interferometer makes it possible to reconstruct the absolute values of its phase shift profile. In practice, the spatial resolution of the reconstruction is determined by the scanning step, while the phase resolution is defined by the fringe spacing $\Lambda$ and the pixel size $\Delta p$ of the high-resolution detector used. Since the fringe spacing corresponds to a phase difference $\Delta\varphi$ equal to $2\pi$ radian [according to Eq. (6)], then the phase resolution can be estimated as $2\pi\ \Delta p\ /\ \Lambda$.

It is worth noting that the phase sensitivity depends on the effective aperture of the CRL located downstream of the sample. Due to the internal structure of the sample, the initial phase difference $\Delta\varphi$ has a variation within the effective aperture, which leads to the aperiodic distribution of the fringes in the interference pattern. Moreover, in some cases, different parts of the sample have a collective effect on the shift of each fringe, which is reflected in distortions in the reconstruction of the phase profile of the sample. It becomes apparent that the proposed imaging technique is more sensitive to samples in which the characteristic dimensions of the inner structure are larger or comparable to the size of the effective aperture. This has been experimentally demonstrated using fibres of different sizes as the test samples.

## 3. Manufacturing and experiment

Planar parabolic bilenses were manufactured using the process involving electron beam lithography and deep etching into silicon [18,19]. A single interferometer is a structure with an etching depth of about 70 µm, which represents two parallel planar arrays of individual double concave parabolic lenses, transversally separated by a distance $d$ equal to 60 µm. Each lens has the physical aperture $A$ of 50 µm while the curvature radius $R$ in the apexes of its parabolic refractive surfaces is 6.25 µm. It should be noted that the measured roughness of the lens surface is in the order of 20 nm, which, does not significantly affect the formation of interference patterns.

A scanning electron microscope image of the bilens interferometers with an indication of their main geometric parameters is shown in Fig. 1. Five sets of bilens are located on the same silicon chip. They differ in the number $N$ of individual parabolic lenses in the array and, as a result, have different focal lengths. Moreover, by choosing suitable bilens, it becomes possible to select the desired effective aperture or reasonably short focal distance at higher X-ray energies. It should be emphasized that five bilenses on a chip allow covering the X-ray energy range from 10 to 50 keV.

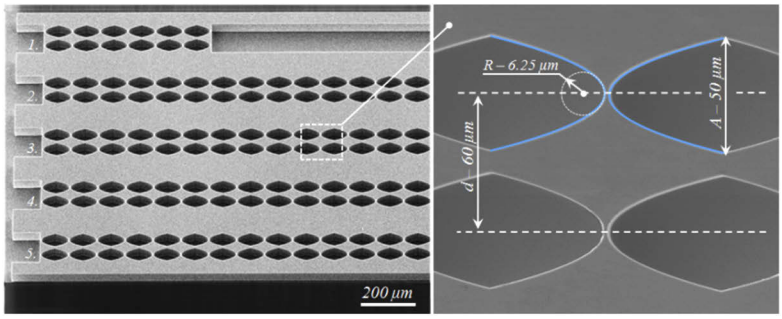


**Fig. 1.** Scanning Electron Microscope image of the planar parabolic bilens interferometers, with the indication of main bilens geometric parameters such as curvature radius $R$, physical aperture $A$ and distance $d$ between two CRLs.

Optics EXPRESS

According to the presented theoretical considerations, the wavelength $\lambda$ has a significant impact on the main optical characteristics of the bilens interferometers and, as a result, on the quality of the formed interference pattern. This refers to the visibility value $V$ and the period $\Lambda$ of the interference fringes. With having this in mind, optimal X-ray energy of 12 keV ($\lambda = 1.033$ Å) was chosen for the experimental demonstration of the phase-sensitive imaging technique. Table 1 summarizes the main parameters of bilens interferometers considered for this energy. For the tests described in this paper, a second bilens interferometer in Table 1 consisting of 26 individual lenses was used. At the energy of 12 keV, the theoretical focal distance $f$ of lenses in the bilens interferometer is 35.5 mm, the effective aperture $A_{eff}$ is 13.2 µm and the expected diffraction-limited focal spot size $\sigma_f$ is to 140 nm.

**Table 1. Main optical characteristics of the bilens interferometers.[a]**

| Bilens number | Number of lenses $N$ | Focal length $f$, mm | Effective aperture $A_{eff}$, µm | Diffraction-limited focal spot size $\sigma_f$, nm |
|---|---|---|---|---|
| 1 | 6 | 154.0 | 27.5 | 290 |
| 2 | 26 | 35.5 | 13.2 | 140 |
| 3 | 58 | 16.0 | 8.8 | 90 |
| 4 | 104 | 8.9 | 7.0 | 70 |
| 5 | 162 | 5.7 | 5.3 | 60 |

[a]The focal distances $f$, effective aperture $A_{eff}$ and diffraction-limited focal spot size $\sigma_f$ are calculated for X-ray energy of 12 keV.

The experimental tests of phase-sensitive imaging technique based on bilens interferometer were performed at the micro-optics test bench of the ESRF undulator beamline ID06. Liquid nitrogen cooled double crystal and fixed exit Si-111 monochromator was used to adjust X-ray energy to 12 keV. To reduce the influence of the third undulator harmonic, the second crystal of the monochromator was slightly detuned from the Bragg position. The detuning angle was around 10 µrad (2 arc. sec.) to provide the remaining fundamental harmonic flux of about 80%.

The bilens system was mounted at a distance of 58 m from the source, on the stage with all necessary for alignment rotation and translation movements. Given the location of the source, the theoretical distance $z_f$ at which the transmitted beams were focused by the bilens, and the space $d_f$ between two foci practically do not differ from the values of $f$ and $d$, respectively. Interference patterns were recorded at a distance of about 3.9 m from the foci using an X-ray high-resolution FReLoN CCD detector. The FReLoN uses an AMTEL chip ($2048 \times 2048$ pixels, 14 mm pixel size, 16 bit), a GGG: Eu scintillator 10 mm thick, and an optical system with total magnification 50 (20x microscope objective and 2.5x eyepiece). The input field of view is $0.573 \times 0.573$ µm with an input pixel size of 0.28 µm. The spatial resolution of the imaging system defined by scintillator and optics is about 0.9 µm (3 pixels). Samples were placed upstream of the interferometer at a distance of about 27 mm. The experimental setup is shown in Fig. 2.

First, we tested the bilens interferometer without samples, recording the interference pattern with the CCD detector. Typical exposure time was 10 seconds during the 7/8 beam bunch mode (200 mA current). The observed interference pattern and its cross-section, which is intensity variation obtained for the line through the center of the fringe pattern, are shown in Fig. 3. The fringes are visible in a vertical direction up to several millimeters, which corresponds to the expected result of about 1.5 mm FWHM envelope of the fringes.

The quality of the fringes produced by bilens can be described quantitatively using the visibility, which in our experimental conditions can be measured as the ratio of the difference to the sum of maximum and adjacent minimum intensity values in the observed interference fringe pattern:

Optics EXPRESS

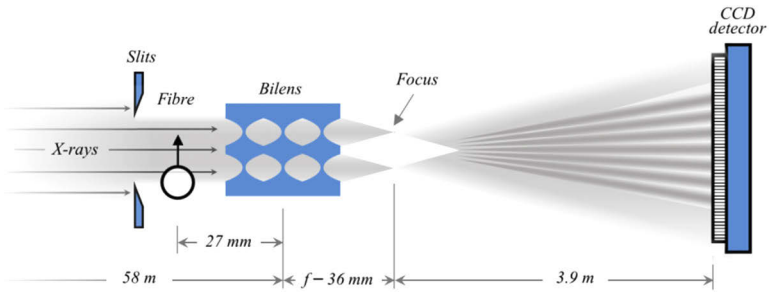


**Fig. 2.** Experimental setup for the phase-sensitive imaging technique based on bilens interferometer. Under coherent X-ray illumination, the bilens forms a periodical pattern of the interference fringes on the CCD detector. The position of the fringes is sensitive to the phase delays of the beam caused by the sample located in front of the bilens.

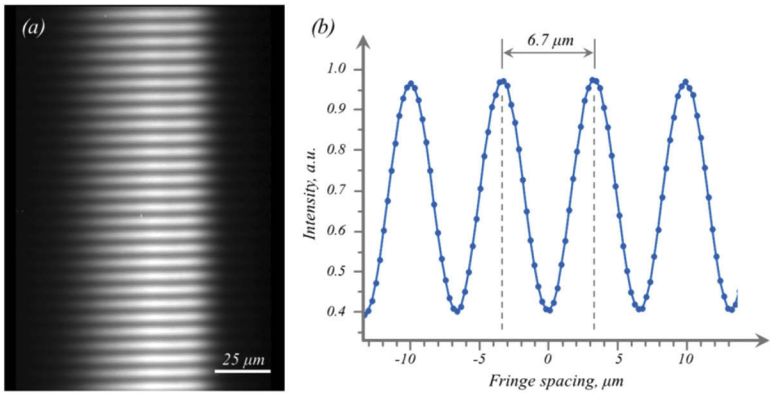


**Fig. 3.** Experimental results of the bilens interferometer test. (a) The observed interference pattern and (b) cross-section representing an intensity variation obtained for the line through the center of the fringes pattern.

$V = (I_{max} - I_{min}) / (I_{max} + I_{min})$. Thus, as can be seen from Fig. 3(b), the fringe visibility was about 42%. Calculations made with Eq. (5) give a vertical source size of about 46 μm, which is very consistent with the size of the source measured using other techniques such as boron fibre or direct imaging of the source with CRLs [20,21]. The measured fringe spacing Λ (peak-to-peak distance) was 6.7 ± 0.1 μm, which is a very good agreement with the calculations given by Eq. (4).

To demonstrate the capabilities of the phase-sensitive imaging method, we selected carbon fibre with a diameter of 9 μm, tungsten fibre with a diameter of 4 μm, and boron fibre, which is a coaxial structure consisting of a boron shell with a diameter of 100 μm and a tungsten core inside with a diameter of 15 μm, as test samples. It should be noted that carbon fibre is a weakly absorbing material, while tungsten fibre is a very absorbing one. As for the boron fibre with a tungsten core, it has both weak and very absorbing components, and, besides, its size is comparable to the full aperture of bilens interferometer.

The fibre scanning process was carried out as follows. First, when moving the fibre perpendicular to the optical axes of the bilens, a set of interference patterns was recorded. Depending on the sample, the scanning step varied from 200 nm up to 1 μm, and the scanning area ranged from 20 to 100 μm. Then, for each fibre position, cross-sections are cut out from the corresponding interference pattern and, combining them, an experimental scan image is formed. This scan image shows the shifts of interference fringes observed during the scanning process, which

Optics EXPRESS

are the result of phase delays of the beam generated by the fibre. The absolute values of the phase delay $\Delta\varphi$ are easily measured from the corresponding values of the shift of the fringes $\Delta x$ [see Eq. (6)]. The spatial resolution of the formed phase reconstruction is determened by the corresponding scan step, while the phase resolution of the proposed imaging technique is about 263 mrad (~$0.08\pi$ rad) for the experimental layout under consideration.

Carbon fibre was scanned with a step of 200 nm, while the scanning area was 20 μm. The experimental scan image for carbon fibre is presented in Fig. 4(a). The shifts of interference fringes appearing during scanning are clearly visible, and for clarity, they are shown as a dashed line in the image. The numerically simulated scan image shown in Fig. 4(b) agrees very well with the experimental result.

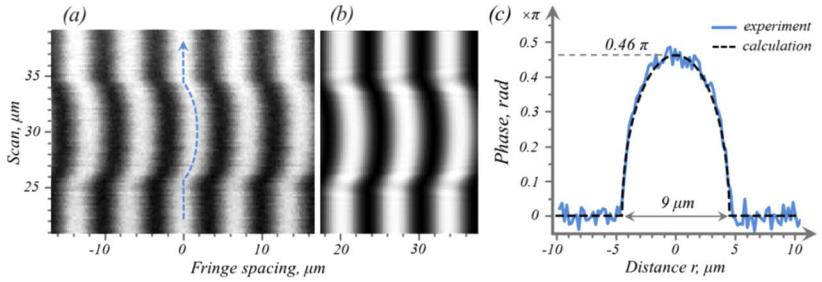


**Fig. 4.** Experimental demonstration of the phase-sensitive imaging technique based on bilens interferometer where the relatively small carbon fibre with a diameter of 9 μm was studied. (a) Experimental and (b) numerically simulated scan images (the fringes shifts during the scan are marked by a dashed line). (c) The reconstruction of the phase profile of the carbon fibre and the corresponding theoretical curve.

Analysis of the experimental scan image allowed reconstructing the phase profile of the sample, which is depicted in Fig. 4(c). The experimentally measured maximum phase shift was $0.46\pi$ and the diameter of the fibre was 9 μm. Thus, a combination of both characteristics corresponds to the theoretical value of refractive index decrement equal to $2.65{\cdot}10^{-6}$ at an energy 12 keV for a carbon fibre with a density of 1.84 g / cm$^3$. It is worth noting the shape of the phase profile of the fibre completely coincides with the theoretical curve for carbon fibre [marked by a dashed line in Fig. 4(c)], calculated by the equation:

$$\Delta\varphi = \frac{2\delta_0(r_0^2 - r^2)^{1/2}}{\lambda}2\pi, \quad |r| \le r_0, \tag{7}$$

where $\delta_0$ is the refractive index decrement of a fibre material, $r_0$ is the fibre radius, $r$ is the radial coordinate.

The excellent sensitivity of the proposed technique to phase variations in carbon fibre is connected primarily with its size, which is comparable with the effective aperture of the bilens CRLs. However, the correct phase reconstruction of samples with smaller sizes can be problematic. To demonstrate the capabilities of the phase determination approach, a tungsten fibre with a small diameter of 4 μm was studied.

Scanning of the tungsten fibre was carried out with the same parameters as the carbon fibre, i.e. the scanning step of 200 nm and the scanning area of 20 μm. Experimental and numerically simulated scan images for tungsten fibre are shown in Figs. 5(a) and 5(b), respectively. It can be seen that both images are qualitatively consistent with each other. However, the result of the reconstruction of the phase profile presented in Fig. 5(c) is slightly inconsistent with the theoretical curve calculated by the Eq. (7). As already mentioned, different parts of the sample have a collective effect on the shift of each fringe. With a sufficiently strong variation in the phase

Optics EXPRESS

delay produced by the sample, this effect becomes noticeable. Thus, significant changes in the phase difference introduced by a small tungsten fibre located within a large effective aperture led to the observed distortion of the phase profile of the sample. Despite this, the measured maximum phase shift of $1.58\pi$ and a fibre diameter of 4 μm allowed to estimate a tungsten refractive index decrement, which coincided with a theoretical value of $2{\cdot}10^{-5}$ at an energy 12 keV.

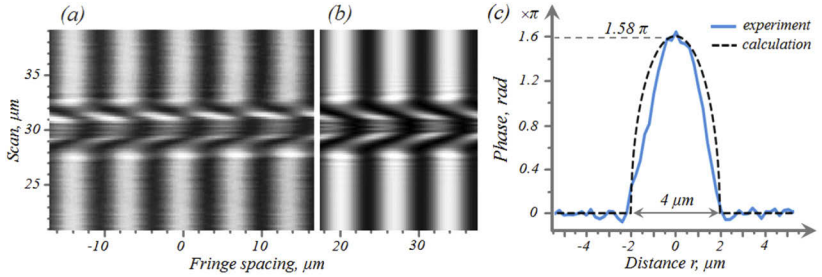


**Fig. 5.** The phase sensitivity study of the proposed imaging technique was carried out using a small tungsten fibre with a diameter of 4 μm. (a) Experimental and (b) numerically simulated scan images. (c) Reconstruction of the phase profile of the tungsten fibre and the corresponding theoretical curve.

Relatively small fibres, the sizes of which do not exceed the distance $d$ between two separated CRLs in the bilens, were considered above. This allowed us to scan each fibre in the beam passing through only one CRL in the bilens, while the second CRL provided a reference beam. In this case, the observed shift of interference fringes directly corresponded to the absolute value of the phase delay. The next test was carried out using 100 μm boron fibre with 15 μm tungsten core. Unlike small fibres, a large boron fibre can overlap both beams. Nevertheless, it is still possible to reconstruct the absolute values of the phase profile using the relative shifts of the fringes obtained by scanning the sample. It is worth noting that the preliminary assessment measurements of the boron fibre were already performed by us [22]. However, in this paper, final and more thorough measurements are presented.

The experimental scan image for boron fibre with a tungsten core is demonstrated in Fig. 6(a). The sample was scanned with a step of 1 μm, and the scanning range was ± 100 μm relative to the bilens centre. In the range from –20 to +20 μm in the scan image, the shift of the fringes is the joint result of the phase delays of the beam caused by the boron fibre, which was in front of both CRLs simultaneously. It should be noted that in this case, the shifts of the fringes are relative, and as before, can be defined by the Eq. (6). However, taking into account the distance $d$ between the CRLs of the bilens, the absolute values of the phase profile of the sample can be reconstructed. The remaining areas correspond to scanning the sample by a beam passing through only one of CRLs. The two dark areas at the scanning positions around –30 and +30 μm are mainly determined by the tungsten core when it was opposite the CRLs apertures during the scanning process. Due to the strong absorption of X-rays by the tungsten core, the contrast of the fringes inside these areas is slightly lower than outside, however, the fringes are still visible.

The observed shifts of the fringes are indicated by a dashed line. During the scan, the fringes are first shifted in one direction by more than five periods relative to the interference fringes without sample, and then symmetrically in the other direction. It is related to the axial symmetry of the fibre. Thus, in the zero position of the scan, when the tungsten core of the fibre is located opposite the centre of bilens, the shift of the fringes is not observed. The numerically simulated scan image shown in Fig. 6(b) is fully consistent with experimental observations.

The reconstruction of the phase profile of boron fibre, taken into account its large size, is presented in Fig. 6(c). The theoretical curve calculated for the expected coaxial structure of the boron fibre, consisting of 15 μm tungsten core and 100 μm boron shell, well describes

Optics EXPRESS

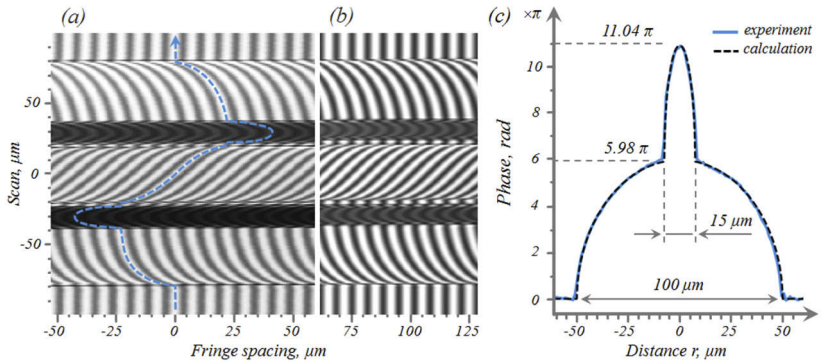


**Fig. 6.** The study of the phase profile of boron fibre, which is a coaxial structure, consisting of a large, weakly absorbing boron shell with a diameter of 100 μm and a small very absorbing tungsten core with a diameter of 15 μm. (a) Experimental and (b) numerically simulated scan images (shifts of the fringes during the scan are marked by a dashed line). (c) Reconstruction of the phase profile of the boron fibre and the corresponding theoretical curve.

the experimental result. Thus, the measured maximum value of the phase shift, equal to $11.04\pi$, corresponds to the joint contribution to the phase delay of boron with a thickness

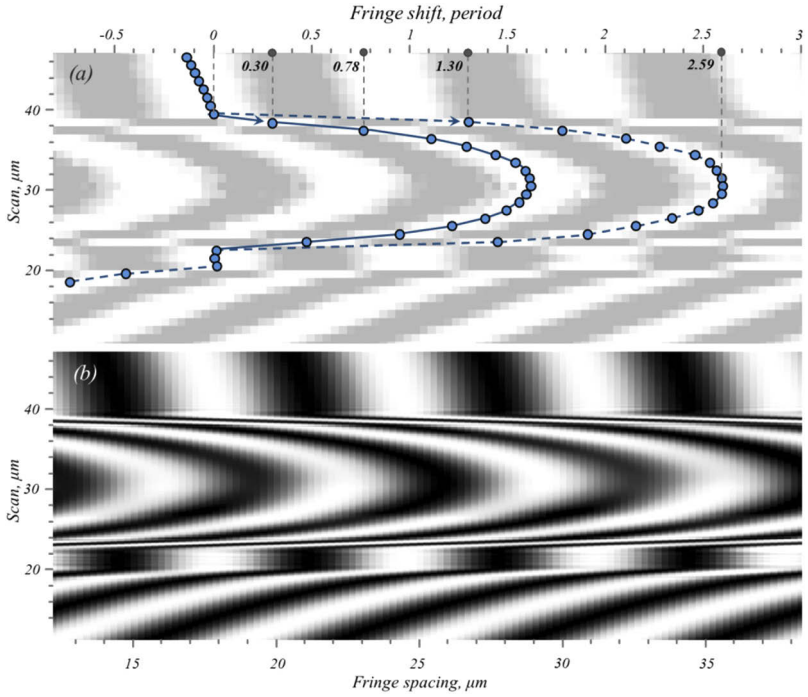


**Fig. 7.** Normalized scan images obtained for the boron fibre in the area of the tungsten core. (a) Experimental scan image with the scanning step of 1 μm. Peaks of the fringes are depicted by round markers. The ambiguity in the detection of the phase shift forming by the boron fibre lies in the choice between the two possible ways, which are marked by solid and dashed lines. (b) Numerically simulated normalized scan image with the scanning step of 50 nm.

Optics EXPRESS

of 100–15 = 75 μm with a refractive index decrement of $3.1 \cdot 10^{-6}$ and 15 μm tungsten with a refractive index decrement of $2 \cdot 10^{-5}$. It is worth noting that for boron with a thickness of 100 μm, the corresponding phase shift will be $5.98\pi$, which was marked on the phase profile for clarity.

To correctly determine the absolute values of the phase shift formed by the sample, it is necessary to choose a scanning step at which the relative shift of the interference fringe in the scan image does not exceed half their period. In this case, the direction and magnitude of the fringe shifts are unambiguously determined. For example, for boron fibre, a maximum phase gradient is formed near the edge of its tungsten core. According to Eq. (7) for the experiments with boron fibre in the existing experimental layout, the scanning step should be less than 100 nm. A spatial resolution of 1 μm, used in the experiment, is insufficient for direct observation of the phase jump at the edge of the tungsten core. The theoretical value of the fringe shift in 1 μm area from the tungsten core edge is about $2.5\pi$ radians or 1.25 period of the fringes (more than half period), which leads to some ambiguity in determining the phase during the reconstruction of the phase profile. However, a logical analysis of the fringe shifts allows for solving this problem.

Figure 7(a) shows a scan image of the boron fibre in the area of the tungsten core, where the maximum and minimum intensities of the fringes formed at each scanning step were normalized. Besides, the fringes are highlighted by the intensity threshold method, and the peaks of the fringes are depicted by round markers. Careful consideration of the scan image gives two ways for the fringe shift determination, which are depicted by a solid and dashed line. Knowing the structure of the sample under study, it is logical to assume that the gradient of the fringe shift in the area of the tungsten core edge should change monotonously. The solid line has a maximum of the derivative in the area of the several scanning steps from the edge while the derivative of the dashed line is permanent decrease. Thus, the shift of the fringe marked by the dashed line seems to be veritable. In addition, in this case, the observed fringe shift on the edge is about $2.6\pi$ radians (1.3 of the period), which corresponds to the theoretical expectation. The numerical simulation of the corresponding scan image performed with a scanning step of 50 nm, also confirms the correctness of this choice [see Fig. 7(b)].

## 4. Conclusion

In this paper, the bilens interferometer based on refractive optics was implemented for phase-sensitive X-ray imaging of weakly absorbing materials in the high energy X-ray domain. The proposed approach allows obtaining the phase profile of the sample with a fairly high phase and spatial resolution by observing the shift of the interference fringes generated by the interferometer during the scanning of the sample across the bilens. The capabilities of the phase-sensitive X-ray imaging technique were studied theoretically and experimentally, as the corresponded computer simulations were presented. The absolute values of the phase profile were reconstructed both for small samples scanned through one CRL and for the large ones that overlap both CRLs in the interferometer. The experimental results are fully consistent with theoretical concepts and the corresponding numerical calculations.

To demonstrate the phase sensitivity of the proposed imaging technique, fibres of different sizes were used as test samples. For relatively small fibres, the sizes of which do not exceed the distance $d$ between two separated CRLs in the bilens, it was possible to scan each fibre in the beam passing through only one CRL in the bilens, while the second CRL provided a reference beam. In this case, the observed shift of interference fringes directly corresponded to the absolute value of the phase delay. For carbon fibre with a diameter of 9 μm, which is comparable with effective aperture $A_{eff}$ of the bilens CRLs, the excellent sensitivity of the proposed technique to phase variations was demonstrated. Using 100 μm boron fibre with 15 μm tungsten core, which was overlapping both beams in the bilens, it was also possible to reconstruct the absolute values of the phase profile by the relative shifts of the interference fringes.

Optics EXPRESS

It was shown that for a tungsten fibre with a diameter of 4 μm, which is smaller than the effective aperture $A_{eff}$ of the bilens CRLs, some distortions were observed in the reconstructed phase profile of the sample. This is due to the aperiodic distribution of the fringes in the interference pattern, caused by a change in the internal structure of the sample within the effective aperture, and also because different parts of the sample have a collective effect on the shift of each fringe. Nevertheless, the latter can be neglected when the distances from the bilens to the sample and from the bilens to the detector recording the interference pattern are bounded by the thin lens formula. In this case, one of the CRLs in the bilens creates an enlarged image of the sample, while the second CRL generates a reference wave for interference. As a result, the fringe shifts of the interference pattern produced by the different parts of the sample are localized in the areas corresponding to their image. This allows reconstructing a sample phase profile without the scanning process, using only one interference pattern. The theoretical minimum sample size, the phase of which can be detected by the proposed approach, is $\gamma A_{eff} = \sigma_f$ which is about 140 nm for the optical system under consideration. An additional increase in phase sensitivity is also possible by using an X-ray microscopy setup by introducing the CRL objective in front of the sample, thereby obtaining the enlarged image of the sample, matching its size to the lens effective aperture.

Knowing that the bilens system generates two diffraction-limited focal spots with the size $\sigma_f$ (up to tens of nm), separated by a distance $d$ of several tens of microns, the sample can be placed in the focal plane $z_f$ of the bilens CRLs. In this case, the small size of the focused beams equal to $\sigma_f$ provides excellent phase sensitivity and high spatial resolutions and also allows to completely avoid possible distortions of the phase reconstruction.

We would like to emphasize that the proposed approach is not only limited by 1D objects but also allows studying of two-dimensional samples, by adding to the scanning of the sample across the bilens, an additional scanning of the sample along the lens axis. To demonstrate this possibility, we carried out a numerical imaging simulation of a silicon sphere with a diameter of 30 μm, having a spherical cavity of an 8 μm diameter placed out of the sample center. The parameters of the simulated layout completely coincide with the experimental conditions considered in this paper. At the same time, the chosen scan steps in both directions across and along the bi-lens system were 200 nm. Numerically simulated scan images obtained at the different positions of the sample, which corresponded to the horizontal positions of the cavity and ball centers are shown in Figs. 8(a) and 8(b), respectively. Analysis of the scan images allows reconstructing the two-dimensional phase shift distribution in the sample [Fig. 8(c)]. The result of numerical calculations demonstrates the extended capabilities of the proposed phase-sensitive approach. It also does not exclude the possibility of a tomographic study of the phase shifts of the samples.

It should be noted that the ability to directly detect the phase shift is an absolute advantage of X-ray interferometric imaging using bilens among other phase-sensitive methods, such as diffraction enhanced imaging (DEI) or Talbot interferometric imaging which detect only the spatial gradient of the phase shifts [23–26]. Furthermore, tracking the change of the shape of the envelope of the interference fringes and their visibility during the scanning of the sample, it possible to obtain the corresponding absorption and scattering profiles. As a result of these advantages, the proposed approach has the highest resolution in density and provides a way to perform precise studies of biomedical and organic samples without using any additional methods for their preparation.

A straightforward method for measuring the effective source size was experimentally demonstrated by analyzing the interference pattern produced by the bilens interferometer. Considering the ongoing transition of modern accelerator X-ray sources to diffraction-limited synchrotrons (MAX IV, ESRF-EBS, PETRA-IV), the development of such methods of source diagnostics is an especially relevant task. Also, the proposed phase-sensitive X-ray imaging technique is an

Optics EXPRESS

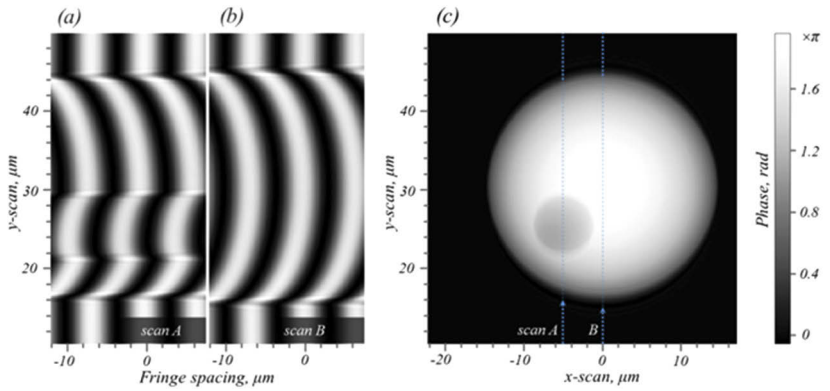


**Fig. 8.** The numerical simulation of a two-dimensional scan process and reconstruction of the phase shift distribution for a silicon ball with a diameter of 30 μm, which has a spherical cavity with a diameter of 8 μm, displaced relative to the sample center. Numerically simulated scan images obtained during *A* and *B* scans corresponding to the positions of the center of the cavity (a) and the ball (b), respectively. (c) Reconstruction of the two-dimensional phase distribution of the sample.

effective tool for phase diagnostics of the wavefront of the synchrotron beam. The transverse phase profile of the beam can be obtained by scanning it with bilens.

In the case of the interferometer consisting of multiple sets of parallel arrays of identical planar refractive lenses, an interference field is produced, which can be described by the Talbot imaging formalism [14,15]. A multilens system generates a set of diffraction-limited (up to tens of nm) focal spots with a period of up to tens of microns, and therefore it can be considered as an analog of a grating interferometer with extremely small gaps, which provides a very thin region of the phase shift integration that the sample can cause. Spatial resolution is determined by the size of the diffraction-limited focal spots created by a multilens interferometer. Moreover, unlike grating interferometers, a multilens interferometer can be used in the hard X-ray region (>30keV), while the manufacturing of a thick micron-pitch grating interferometer is problematic. These advantages of the multilens interferometers open up new opportunities both for phase-contrast X-ray imaging techniques and for X-ray interferometry in general.

## Funding

Russian Science Foundation (19-72-30009).

## Acknowledgments

The authors are very grateful to C. Detlefs and P. Wattecamps for their help during the experiments at the ID 06 beamline. The authors thank the Russian Academic Excellence Project at the Immanuel Kant Baltic Federal University for funding travel and accommodation for X-ray tests.

## Disclosures

The authors declare no conflicts of interest.

## References

1. W. Leitenberger, S. M. Kuznetsov, and A. Snigirev, "Interferometric measurements with hard X-rays using a double slit," Opt. Commun. **191**(1-2), 91–96 (2001).

Optics EXPRESS


2. D. Paterson, B. E. Allman, P. J. McMahon, J. Lin, N. Moldovan, K. A. Nugent, I. McNulty, C. T. Chantler, C. C. Retsch, T. H. K. Irving, and D. C. Mancini, "Spatial coherence measurement of X-ray undulator radiation," Opt. Commun. **195**(1-4), 79–84 (2001).
3. W. Leitenberger, H. Wendrock, L. Bischoff, and T. Weitkamp, "Pinhole interferometry with coherent hard X-rays," J. Synchrotron Radiat. **11**(2), 190–197 (2004).
4. M. Lyubomirskiy, I. Snigireva, and A. Snigirev, "Lens coupled tunable Young's double pinhole system for hard X-ray spatial coherence characterization," Opt. Express **24**(12), 13679 (2016).
5. K. Fezzaa, F. Comin, S. Marchesini, R. Coïsson, and M. Belakhovsky, "X-ray interferometry at ESRF using two coherent beams from fresnel mirrors," J. X-Ray Sci. Technol. **7**(1), 12–23 (1997).
6. W. Leitenberger and U. Pietsch, "A monolithic Fresnel bimirror for hard X-rays and its application for coherence measurements," J. Synchrotron Radiat. **14**(2), 196–203 (2007).
7. M. Lyubomirskiy, I. Snigireva, S. Kuznetsov, V. Yunkin, and A. Snigirev, "Hard x-ray single crystal bi-mirror," Opt. Lett. **40**(10), 2205–2208 (2015).
8. A. R. Lang and A. P. W. Makepeace, "Production of synchrotron X-ray biprism interference patterns with control of fringe spacing," J. Synchrotron Radiat. **6**(2), 59–61 (1999).
9. Y. Suzuki, "Measurement of x-ray coherence using two-beam interferometer with prism optics," Rev. Sci. Instrum. **75**(4), 1026–1029 (2004).
10. C. David, B. Nöhammer, H. H. Solak, and E. Ziegler, "Differential x-ray phase contrast imaging using a shearing interferometer," Appl. Phys. Lett. **81**(17), 3287–3289 (2002).
11. A. Momose, S. Kawamoto, I. Koyama, Y. Hamaishi, K. Takai, and Y. Suzuki, "Demonstration of x-ray Talbot interferometry," Jpn. J. Appl. Phys. **42**(Part 2, No. 7B), L866–L868 (2003).
12. F. Pfeiffer, C. Kottler, O. Bunk, and C. David, "Hard X-ray phase tomography with low-brilliance sources," Phys. Rev. Lett. **98**(10), 108105 (2007).
13. A. Snigirev, I. Snigireva, V. Kohn, V. Yunkin, S. Kuznetsov, M. B. Grigoriev, T. Roth, G. Vaughan, and C. Detlefs, "X-ray nanointerferometer based on Si refractive bilenses," Phys. Rev. Lett. **103**(6), 064801 (2009).
14. A. Snigirev, I. Snigireva, M. Lyubomirskiy, V. Kohn, V. Yunkin, and S. Kuznetsov, "X-ray multilens interferometer based on Si refractive lenses," Opt. Express **22**(21), 25842 (2014).
15. M. Lyubomirskiy, I. Snigireva, V. Kohn, S. Kuznetsov, V. Yunkin, G. Vaughan, and A. Snigirev, "30-Lens interferometer for high-energy X-rays," J. Synchrotron Radiat. **23**(5), 1104–1109 (2016).
16. A. Snigirev, V. Kohn, I. Snigireva, and B. Lengeler, "A compound refractive lens for focusing high-energy X-rays," Nature **384**(6604), 49–51 (1996).
17. V. G. Kohn, "Effective aperture of X-ray compound refractive lenses," J. Synchrotron Radiat. **24**(3), 609–614 (2017).
18. V. Aristov, M. Grigoriev, S. Kuznetsov, L. Shabelnikov, V. Yunkin, T. Weitkamp, C. Rau, I. Snigireva, A. Snigirev, M. Hoffmann, and E. Voges, "X-ray refractive planar lens with minimized absorption," Appl. Phys. Lett. **77**(24), 4058–4060 (2000).
19. A. Snigirev, I. Snigireva, M. Grigoriev, V. Yunkin, M. Di Michiel, S. Kuznetsov, and G. Vaughan, "Silicon planar lenses for high-energy x-ray nanofocusing," Proc. SPIE **6705**, 670506 (2007).
20. V. Kohn, I. Snigireva, and A. Snigirev, "Direct measurement of transverse coherence length of hard x rays from interference fringes," Phys. Rev. Lett. **85**(13), 2745–2748 (2000).
21. T. Weitkamp, O. Chubar, M. Drakopoulos, A. Souvorov, I. Snigireva, A. Snigirev, F. Günzler, C. Schroer, and B. Lengeler, "Refractive lenses as a beam diagnostics tool for high-energy synchrotron radiation," Nucl. Instrum. Methods Phys. Res., Sect. A **467-468**, 248–251 (2001).
22. D. Zverev, I. Snigireva, V. Kohn, S. Kuznetsov, V. Yunkin, and A. Snigirev, "X-ray Phase Contrast Imaging Technique Using Bilens Interferometer," Microsc. Microanal. **24**(S2), 164–165 (2018).
23. E. Pagot, S. Fiedler, P. Cloetens, A. Bravin, P. Coan, K. Fezzaa, J. Baruchel, and J. Härtwig, "Quantitative comparison between two phase contrast techniques: Diffraction enhanced imaging and phase propagation imaging," Phys. Med. Biol. **50**(4), 709–724 (2005).
24. P. C. Diemoz, A. Bravin, and P. Coan, "Theoretical comparison of three X-ray phase-contrast imaging techniques: propagation-based imaging, analyzer-based imaging and grating interferometry," Opt. Express **20**(3), 2789 (2012).
25. T. Zhou, U. Lundström, T. Thüring, S. Rutishauser, D. H. Larsson, M. Stampanoni, C. David, H. M. Hertz, and A. Burvall, "Comparison of two x-ray phase-contrast imaging methods with a microfocus source," Opt. Express **21**(25), 30183 (2013).
26. Y. Akio, W. Jin, H. Kazuyuki, and T. Tohoru, "Quantitative comparison of imaging performance of x-ray interferometric imaging and diffraction enhanced imaging," Med. Phys. **35**(10), 4724–4734 (2008).